AIAA JOURNAL
Vol. 47, No. 10, October 2009

# Statistical Combination of Time-Varying Loads

B. H. Sako,* A. M. Kabe,† and S. S. Lee‡
*The Aerospace Corporation, Los Angeles, California 90009-2957*

DOI: 10.2514/1.39384

**The total responses experienced by a system are often due to distinct and independent contributors. For example, during atmospheric flight a launch vehicle and its spacecraft will experience loads from sources such as dynamic pressure, turbulence/gust, buffet, and thrust oscillation and vectoring. Because of the complexity of the phenomena, each contributor must be established in separate analyses. To obtain a total, the separate results must be combined. There are several combination equations, and three of these are assessed herein by means of Monte Carlo simulations and mathematical analysis. It will be demonstrated that the equation based on the envelope functions of Gaussian response time histories provides a reasonable bound and that the form of the equation in which all contributors are root-sum-squared will frequently underpredict the correct total.**

## Nomenclature

| | | |
|---|---|---|
| $\mathbf{B}(t)$ | = | vector-valued function of buffet load time histories |
| $\ddot{b}_{x;i,j}(t)$ | = | base excitation to first single-degree-of-freedom system for $i$th loads-combination-equation run and $j$th Monte Carlo draw |
| $\ddot{b}_{y;i,j}(t)$ | = | base excitation to second single-degree-of-freedom system for $i$th loads-combination-equation run and $j$th Monte Carlo draw |
| CLT | = | central-limit-theorem-based loads combination equation |
| ENV | = | envelope-function-based loads combination equation |
| $F_x(\cdot)$ | = | cumulative distribution function of $x$ |
| $\bar{f}$ | = | natural frequencies of single-degree-of-freedom system, Hz |
| $f_x(\cdot)$ | = | probability density function of $x$ |
| $G$ | = | one-sided power spectral density, $g^2/\text{Hz}$ |
| $\mathbf{G}(t)$ | = | vector-valued function of gust load time histories |
| $k$ | = | $k$ factor corresponding to a specified enclosure/confidence level |
| $m_n$ | = | $n$th spectral moment |
| $N^+$ | = | expected number of positive maxima for a given duration |
| $p$ | = | enclosure probability |
| $Q$ | = | quality factor for single-degree-of-freedom systems |
| RSS | = | root-sum-square-based loads combination equation |
| $r_{\text{ENV}}$ | = | envelope-function loads-combination-equation ratio |
| $r_{\text{RSS}}$ | = | root-sum-squared loads-combination-equation ratio |
| $r_y$ | = | frequency ratio of narrowband responses, $\bar{f}_y/\bar{f}_x$ |
| $T$ | = | time duration, s |
| $\mathbf{TO}(t)$ | = | vector-valued function of thrust-oscillation load time histories |
| $t$ | = | time, s |
| $u$ | = | sum of the envelopes |
| $\hat{W}_{i,99/90}$ | = | 99/90 estimate of the sum of the peaks $\hat{w}_{i,j}$ over index $j$ |
| $\hat{w}_{i,j}$ | = | sum of the peaks, equal to $\hat{x}_{i,j} + \hat{y}_{i,j}$ |
| $\hat{X}_{i,99/90}$ | = | 99/90 estimate of peak responses $\hat{x}_{i,j}$ over index $j$ |
| $x_i$ | = | $i$th random variable |
| $\hat{x}_i$ | = | $i$th peak of random variable $x_i$ |
| $\hat{x}_{i,j}$ | = | maximum of $\ddot{x}_{i,j}(t)$ |
| $\ddot{x}_{i,j}(t)$ | = | response of first single-degree-of-freedom system for $i$th loads-combination-equation run and $j$th Monte Carlo draw |
| $\tilde{x}(t)$ | = | envelope function of response $x(t)$ |
| $\hat{Y}_{i,99/90}$ | = | 99/90 estimate of peak responses $\hat{y}_{i,j}$ over index $j$ |
| $\hat{y}_{i,j}$ | = | maximum of $\ddot{y}_{i,j}(t)$ |
| $\ddot{y}_{i,j}(t)$ | = | response of second single-degree-of-freedom system for $i$th loads-combination-equation run and $j$th Monte Carlo draw |
| $\hat{Z}_{i,99/90}$ | = | 99/90 estimate of the peaks of the sum $\hat{z}_{i,j}$ over index $j$ |
| $\hat{z}_{i,j}$ | = | maximum of $\ddot{z}_{i,j}(t)$ |
| $\ddot{z}_{i,j}(t)$ | = | total response $\ddot{x}_{i,j}(t) + \ddot{y}_{i,j}(t)$, for $i$th loads-combination-equation run and $j$th Monte Carlo draw |
| $\alpha$ | = | gain factor applied to response $y(t)$ |
| $\Delta f$ | = | bandwidth of narrowband response, Hz |
| $\varepsilon$ | = | Cartwright–Lonquet–Higgins probability distribution parameter |
| $\mu$ | = | mean of a random variable |
| $\hat{\mu}_{x,i}$ | = | sample mean of $\hat{x}_i$ |
| $\nu$ | = | variable of integration |
| $\xi_p$ | = | $p$ quantile corresponding to a normalized Rayleigh distribution |
| $\sigma$ | = | standard deviation of a random variable |
| $\omega$ | = | circular frequency, rad/s |
| $+$ | = | positive maxima |

*Subscript*

| | | |
|---|---|---|
| $H$ | = | Hilbert transform |

*Superscripts*

| | | |
|---|---|---|
| $\hat{}$ | = | peaks or maxima |
| $\tilde{}$ | = | envelope function |

## Introduction

DURING atmospheric flight, a launch vehicle and its payload will experience severe structural loading from multiple sources [1–4]. Loads due to that portion of the vehicle's angle of attack that vary relatively slowly (and hence do not excite the elastic modes of vibration) are often referred to as wind-only, or static-aeroelastic, loads. Loads that are due to the more rapidly changing, nonpersistent wind features are referred to as turbulence and/or gust loads. Loads

Received 26 June 2008; revision received 6 February 2009; accepted for publication 22 February 2009. 

*Distinguished Scientist, Structural Mechanics Subdivision, P.O. Box 92957/M4-911. Senior Member AIAA.

†Associate Principal Director, Structural Mechanics Subdivision, P.O. Box 92957/M4-899. Associate Fellow AIAA.

‡Senior Engineering Specialist, Structural Dynamics Department, P.O. Box 92957/M4-909.

due to the formation of shock waves, shock wave oscillations, flow separation, attached turbulent boundary layers, and the interaction between these phenomena are referred to as buffet loads. In addition, a launch vehicle's liquid engines and/or solid rocket motors also induce slowly varying and vibratory loads.

For many launch vehicles, structural reliability requirements can only be met by restricting the winds through which they are allowed to fly [5–9]. For these vehicles, the predicted flight loads and whether the vehicle will be allowed to launch will not be known until additional analyses are performed just before launch.

The day-of-launch analyses often include developing a steering profile that minimizes the launch vehicle's angle of attack relative to the winds measured close to the launch window. The vehicle is then analytically flown through the measured wind, and static-aeroelastic loads are computed. The static-aeroelastic loads are then combined with the previously calculated turbulence/gust, buffet, and nondeterministic thrust-induced loads [10–14]. Loads due to the difference between the nominal parameters assumed in the analyses and those of the actual vehicle as flown and loads due to the expected change in the wind from the time it is measured to when the vehicle is launched are also included.

Combination of load contributors can be accomplished by means of either a Monte Carlo combination of computed time histories, a Monte Carlo combination of loads drawn from appropriate distributions, or a loads combination equation (LCE). Figure 1 illustrates how Monte Carlo analyses can be used to simulate the flight experience of a single launch vehicle a large number of times and hence is a reasonably accurate analytical means of establishing statistical loads. However, the computational burden can be such that more efficient approaches are used during design loads analyses and during the time-critical day-of-launch analyses. The purpose of this work is to assess three loads combination equations by comparison with Monte Carlo analyses and to better understand the properties of the equations by means of simulations and mathematical analysis.

## Loads Combination Equations

We begin with the central limit theorem [15]. If $x_1, x_2, \ldots, x_i, \ldots, x_n$ are independent variables having distributions with means $\mu_i$ and finite variance $\sigma_i^2$, then for large $n$, the distribution of a new random variable $z$, given by

$$z = \sum_i x_i$$

approaches a Gaussian distribution, with mean

$$\mu_z = \sum_i \mu_i$$

and variance

$$\sigma_z^2 = \sum_i \sigma_i^2$$

The enclosure level of $z$ can then be computed as

$$Z_{k\sigma} = \mu_z + k\sqrt{\sigma_z^2} = \sum_i \mu_i + k\sqrt{\sum_i \sigma_i^2} = \sum_i \mu_i + \sqrt{\sum_i (k\sigma_i)^2} \tag{1}$$

In Eq. (1), $k$ can be selected to yield the desired enclosure level. If we have a finite number of contributors that do not have the same statistical distributions, as is the case for many loads events, then $k$ will not be the same for each contributor for a given enclosure and confidence level, and Eq. (1) can only be applied in an approximate manner:

$$Z_{k\sigma} \approx \sum_i \mu_i + \sqrt{\sum_i (k_i\sigma_i)^2} \tag{2}$$

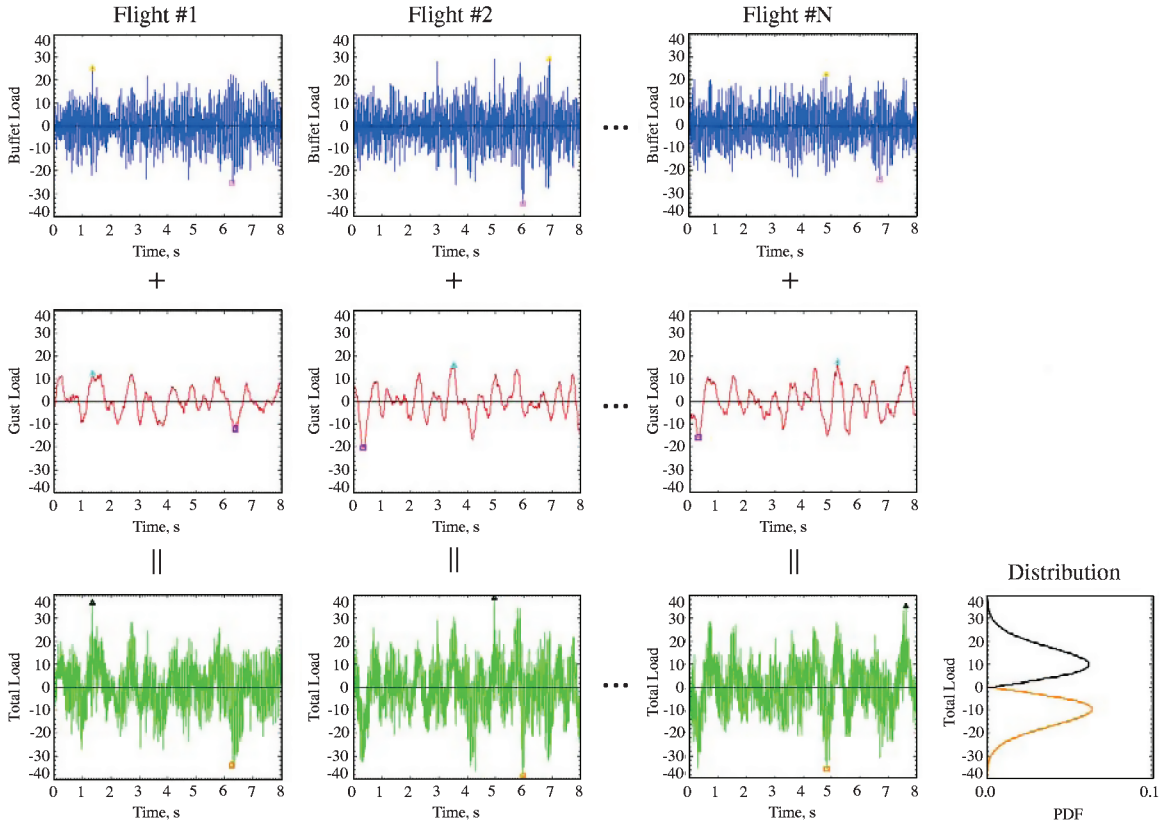


**Fig. 1 In determining expected flight loads that can occur over a short period of time (e.g., during the transonic time of flight), the quantities of most interest are the statistical descriptions of peak positive and peak negative values. Monte Carlo analyses can be used to simulate flight experience of a single launch vehicle a large number of times and establish statistical loads. The resulting distributions have nonzero means.**

Load contributors for finite populations must be established as enclosures with associated confidence levels. Therefore, the dispersed portion of each contributor must be approximated as

$$k_i\sigma_i = \hat{X}_{i,99/90} - \mu_i \tag{3}$$

In Eq. (3), for illustration purposes, $\hat{X}_{i,99/90}$ represents the 99% enclosure, 90% confidence level (99/90) of the load parameter $\hat{X}_i$.

Throughout the paper we will use an enclosure level of 99% with 90% confidence. This will be done for consistency and comparison purposes only. Any other enclosure and confidence level could have been chosen, and in actual application, the enclosure and confidence levels are established by a system's reliability requirements and sample sizes.

Three forms of Eq. (2) will be assessed. The first, which we will refer to as the root-sum-squared (RSS) combination equation, is obtained by assuming that the mean term is zero and that all contributors are dispersed:

$$\text{RSS}\,(\hat{X}_{1,99/90},\ldots,\hat{X}_{n,99/90}) = \sqrt{\sum_{i=1}^{n}\hat{X}_{i,99/90}^2} \tag{4}$$

The second equation, which we will refer to as the central limit theorem (CLT) combination equation, is obtained by establishing the means $\hat{\mu}_i$ and dispersed portions from the distributions of the peaks of the contributors:

$$\text{CLT}\,(\hat{X}_{1,99/90},\ldots,\hat{X}_{n,99/90}) = \sum_{i=1}^{n}\hat{\mu}_i + \sqrt{\sum_{i=1}^{n}(\hat{X}_{i,99/90}-\hat{\mu}_i)^2} \tag{5}$$

The third equation, which we will refer to as the envelope-function (ENV) combination equation, is obtained by developing the means $\tilde{\mu}_i$ from the envelope functions of the time histories. For a discrete Gaussian time series, the envelope function can be calculated using the discrete Fourier transform (see the Appendix for details). The dispersed portion of each load is obtained by subtracting its mean from the corresponding enclosure:

$$\text{ENV}\,(\hat{X}_{1,99/90},\ldots,\hat{X}_{n,99/90}) = \sum_{i=1}^{n}\tilde{\mu}_i + \sqrt{\sum_{i=1}^{n}(\hat{X}_{i,99/90}-\tilde{\mu}_i)^2} \tag{6}$$

For a narrowband response to zero-mean Gaussian excitation, the envelope function and the time-history peaks will have Rayleigh probability density functions [16,17]. The mean will be given by $\sqrt{\pi/2}\,\sigma$, where $\sigma$ is the rms value of the time history. Therefore,

$$\tilde{\mu}_i = \sqrt{\frac{\pi}{2}}\sigma_i \tag{7}$$

It will be shown later that the preceding formulations (6) and (7) will also yield bounding results for the response of multi-degree-of-freedom systems.

To help clarify the various definitions, Fig. 2 shows a typical narrowband response time history, its envelope function, and the peak value. The figure also shows the probability density functions of the time history and envelope function. As can be seen, and as will be demonstrated later, the time-history data points are Gaussian-distributed, and the envelope function has a Rayleigh distribution.

## Monte Carlo Simulations

The three loads combination equations described previously were assessed by means of Monte Carlo simulations of simple systems and a complex spacecraft. For the simple systems, each Monte Carlo simulation combined acceleration time histories from two independent single-degree-of-freedom (SDOF) systems. For the complex spacecraft system, turbulence/gust, buffet, and thrust-oscillation load time histories were computed and combined. We add that the forcing functions, and hence responses in these simulations, were essentially Gaussian. From each Monte Carlo simulation, the 99/90 tolerance bounds of the individual and combined peak responses were determined. These were then compared with the estimates obtained with the three combination equations.

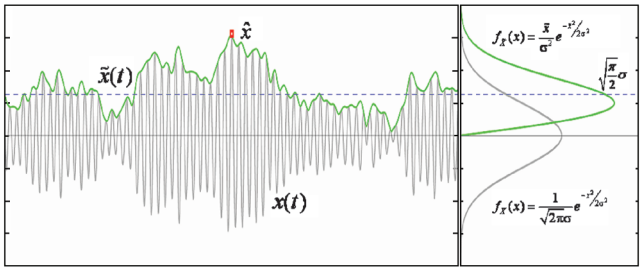


**Fig. 2 Typical narrowband response time history and its envelope function. The peak value is also indicated. The distributions of the time history and its envelope function are also shown.**

### Simple Systems

The statistics of the individual and combined responses from two SDOF systems that were base-excited with broadband Gaussian input formed the basis for the simple system's Monte Carlo simulations. LCE simulation cases were conducted to investigate the effects of frequency separation, amplitude differences, and time duration. The SDOF system that produced the low-frequency response $\ddot{x}(t)$ had a natural frequency that was fixed at 5 Hz for all simulations. The second system's natural frequency $\bar{f}_y$ was set to 6, 11, 19, or 37 Hz, depending on the study being performed. The response of the second system is designated $\ddot{y}(t)$. Damping was set to 1% of critical for both oscillators. The broadband, zero-mean, Gaussian excitation $\ddot{b}_x(t)$ and $\ddot{b}_y(t)$ were uncorrelated and had variance equal to unity. To simulate the effects of combining responses having different relative magnitudes, $\ddot{x}(t)$ and $\ddot{y}(t)$ were first normalized to have unit variance by scaling them by the theoretical $\sigma$ given by Miles's equation [17]:

$$\sigma = \sqrt{\frac{\pi}{2}\bar{f}QG} \tag{8}$$

Then a gain factor $\alpha$ was multiplied to the normalized $\ddot{y}(t)$. For each case, $\alpha$ was defined to be 0.1, 0.25, 0.5, 1, 2, 4, or 10. In Eq. (8), $Q = 50$ corresponds to 1% damping, and $G = 0.002$ g$^2$/Hz is the one-sided power spectral density (PSD) level of the base input having unit variance and sample rate equal to 1000 samples/second. To determine the effects of time duration $T$, LCE cases having $T$ equal to 0.5, 1, 2, 4, 8, or 16 s were performed. Hence, by considering all possible combinations of $\bar{f}_y$, $\alpha$, and $T$, a total of $4 \times 7 \times 6 = 168$ LCE cases were investigated.

For each LCE case in which $\bar{f}_y$, $\alpha$, and $T$ were fixed, the statistics of the LCEs were established by performing 1000 Monte Carlo simulations. Each Monte Carlo simulation (indexed by $i$) consisted of 3000 randomly generated (indexed by $j$) base excitations $\ddot{b}_{x;i,j}(t)$ and $\ddot{b}_{y;i,j}(t)$. The responses $\ddot{x}_{i,j}(t)$ and $\ddot{y}_{i,j}(t)$ were numerically calculated by Duhamel's method. The sum of the responses $\ddot{z}_{i,j}(t) = \ddot{x}_{i,j}(t) + \ddot{y}_{i,j}(t)$ represents the combined or total response. For the $j$th draw, the following peak responses were calculated:

$$\hat{x}_{i,j} = \max_{0\le t\le T}(\ddot{x}_{i,j}(t)), \qquad \hat{y}_{i,j} = \max_{0\le t\le T}(\ddot{y}_{i,j}(t))$$
$$\hat{z}_{i,j} = \max_{0\le t\le T}(\ddot{z}_{i,j}(t)), \qquad \hat{w}_{i,j} = \hat{x}_{i,j} + \hat{y}_{i,j} \tag{9}$$

For the $i$th LCE run, the 99/90 tolerance bounds of the peak responses were determined using ordered statistics:

$$\hat{X}_{i,99/90} = 99/90_{1\le j\le 3000}\{\hat{x}_{i,j}\}, \quad \hat{Y}_{i,99/90} = 99/90_{1\le j\le 3000}\{\hat{y}_{i,j}\}$$
$$\hat{Z}_{i,99/90} = 99/90_{1\le j\le 3000}\{\hat{z}_{i,j}\}, \quad \hat{W}_{i,99/90} = 99/90_{1\le j\le 3000}\{\hat{w}_{i,j}\} \tag{10}$$

Herein, we shall simply refer to $\hat{Z}_{i,99/90}$ as the 99/90 *total load*, and to $\hat{z}$ and $\hat{w}$ as the *peak of the sum* and *sum of the peaks*, respectively.

For the CLT form of the LCE, the means of the peak responses were estimated by the sample means:

$$\hat{\mu}_{x,i} = \frac{1}{3000}\sum_{j=1}^{3000}\hat{x}_{i,j}, \qquad \hat{\mu}_{y,i} = \frac{1}{3000}\sum_{j=1}^{3000}\hat{y}_{i,j} \tag{11}$$

The LCEs for the $i$th run were then calculated as

$$\mathrm{RSS}\,(\hat{X}_{i,99/90}, \hat{Y}_{i,99/90}) = \sqrt{\hat{X}^2_{i,99/90} + \hat{Y}^2_{i,99/90}} \tag{12}$$

$$\mathrm{CLT}(\hat{X}_{i,99/90}, \hat{Y}_{i,99/90}) = \hat{\mu}_{x,i} + \hat{\mu}_{y,i} + \sqrt{(\hat{X}_{i,99/90} - \hat{\mu}_{x,i})^2 + (\hat{Y}_{i,99/90} - \hat{\mu}_{y,i})^2} \tag{13}$$

$$\mathrm{ENV}(\hat{X}_{i,99/90}, \hat{Y}_{i,99/90}) = \sqrt{\frac{\pi}{2}}(1+\alpha) + \sqrt{\left(\hat{X}_{i,99/90} - \sqrt{\frac{\pi}{2}}\right)^2 + \left(\hat{Y}_{i,99/90} - \sqrt{\frac{\pi}{2}}\alpha\right)^2} \tag{14}$$

For each LCE case, histograms of the probability density functions (PDFs) of $\hat{x}$, $\hat{y}$, $\hat{z}$, and $\hat{w}$ were calculated and plotted. Figure 3 shows the results of a simulation for $\bar{f}_y = 37$ Hz, $\alpha = 1.0$, and $T = 8$ s. The histograms and PDFs were scaled so that their locations along the abscissa could be compared easily. Observe that because the sum of peaks bounds the peak of the sum, the PDF of $\hat{w}$ lies to the right of the PDF corresponding to $\hat{z}$. As expected, the histogram of the 99/90 total loads, $\hat{Z}_{i,99/90}$, lies essentially to the right of the 99 percentile, $\hat{Z}_{99\%}$. Also shown are the histograms corresponding to the 1000 RSS, ENV, and CLT LCE estimates. Although the ENV LCE reasonably bounds $\hat{Z}_{i,99/90}$, the RSS LCE estimates underpredict not only the 99/90 estimates $\hat{Z}_i$ but also $\hat{Z}_{99\%}$. On the other hand, we see that the CLT LCE conservatively bounds the 99/90 total loads. In fact, the CLT LCE essentially provides 99/90 estimates of the sum of peaks, $\hat{W}_{i,99/90}$.

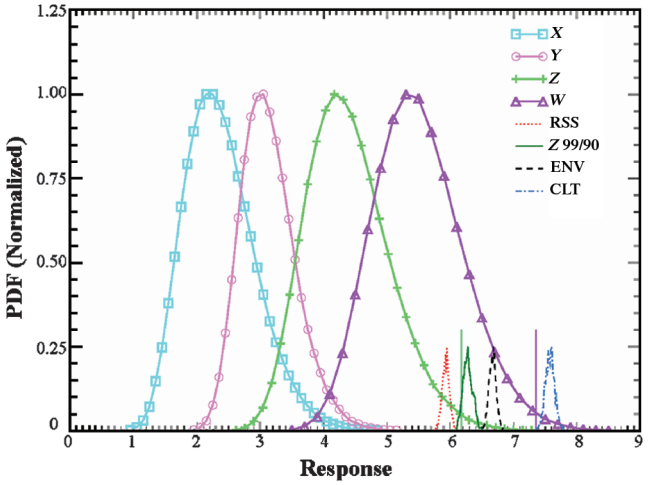


**Fig. 3 Probability density functions of peak responses and LCE histograms for $\bar{f}_y = 37$ Hz, $\alpha = 1$, and $T = 8$ s. PDFs and histograms are scaled for clarity. Light-blue squares, pink circles, green pluses, and purple triangle curves correspond to the PDFs of $\hat{x}$, $\hat{y}$, $\hat{z}$, and $\hat{w}$, respectively. The vertical lines represent the 99 percentiles of the peak $\hat{z}$ and $\hat{w}$ responses.**

Because the LCE is intended to be a tool that combines the statistical responses from various loads events, it is prudent that the LCE provide, in effect, a bound of the 99/90 total loads from the Monte Carlo simulation. For this purpose, the following LCE ratios with respect to $\hat{Z}_{i,99/90}$ were compared:

$$\frac{\mathrm{RSS}(\hat{X}_{i,99/90}, \hat{Y}_{i,99/90})}{\hat{Z}_{i,99/90}}, \qquad \frac{\mathrm{ENV}(\hat{X}_{i,99/90}, \hat{Y}_{i,99/90})}{\hat{Z}_{i,99/90}}$$
$$\frac{\mathrm{CLT}(\hat{X}_{i,99/90}, \hat{Y}_{i,99/90})}{\hat{Z}_{i,99/90}} \tag{15}$$

Figure 4 compares the average LCE ratios for $\bar{f}_y = 37$ Hz, $T = 8$ s, and $\alpha$ varying over the values 0.1, 0.25, 0.5, 1, 2, 4, and 10. For these cases, the RSS form of the LCE underpredicts the 99/90 total loads, whereas the ENV and CLT LCEs provide bounding estimates. Observe that the extremum of each curve occurs when $\alpha \approx 1.0$: that is, when responses of comparable magnitude are being combined. For $\alpha \approx 1$, the RSS LCE had the greatest underprediction with an average of about 6%. The ENV LCE provided a bound that, on average, is 2–6% conservative. The CLT LCE produced more conservative estimates of $\hat{Z}_{i,99/90}$, exceeding the target values by 5–21%.

As can also be ascertained from Fig. 4, the three forms of the LCE considered herein are consistent in that their ratios approach unity as one of the response contributors becomes dominant. This behavior is evident in plots of the average LCE ratios and can be ascertained from the functional form of the LCEs. Moreover, it provides us with a simple requirement on the form of the LCE, and allows us to rule out other LCEs that violate this constraint. For example, an LCE that is defined by increasing the RSS by a scale factor would be inadmissible.

To illustrate the variability of the Monte Carlo results, Fig. 5 shows the LCE ratios for all 1000 simulations for the case $\bar{f}_y = 37$ Hz, $\alpha = 1$, and $T = 8$ s. The results indicate that the random seed used to initiate the Monte Carlo runs can produce about 5% variability in the results with respect to the 99/90 total loads. Observe that the RSS form of the LCE consistently underpredicted the Monte Carlo results (and in some cases, by as much as 10%). On the other hand, the ENV and CLT LCEs provided bounding results with no underpredictions. We add that over all 168 cases and 1000 LCE runs, the ENV form of the LCE did not underpredict the 99/90 total load. Figure 6 presents the standard deviations of the LCE ratios for $\bar{f}_y = 37$ Hz and $T = 8$ s, and for this case, the greatest variability occurs when combining loads of comparable magnitudes.

Figure 7 shows the effects of frequency separation. The average LCE ratios for $T = 8$ s as a function of $\alpha$ are shown for $\bar{f}_y = 6$, 11,

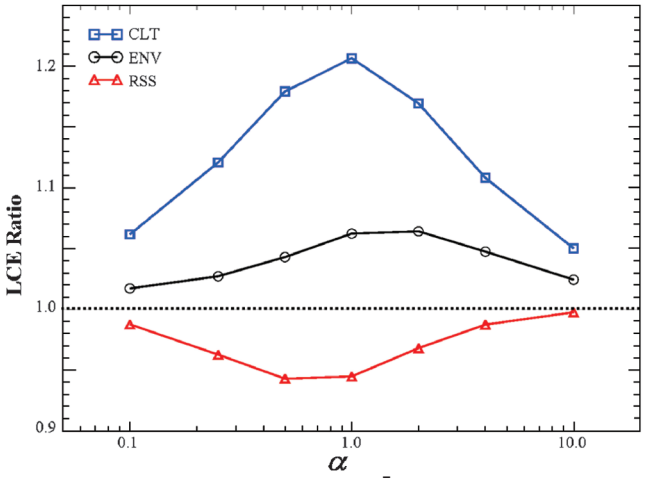


**Fig. 4 Average LCE ratios vs $\alpha$ for $\bar{f}_y = 37$ Hz and $T = 8$ s.**

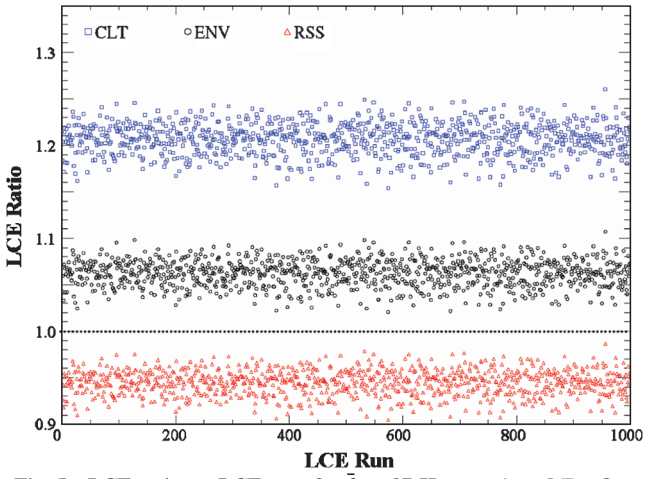


Fig. 5 LCE ratios vs LCE runs for $\bar{f}_y = 37$ Hz, $\alpha = 1$, and $T = 8$ s.

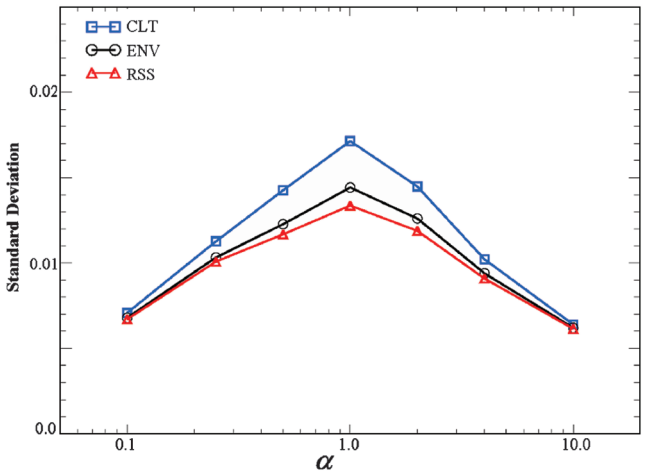


Fig. 6 Standard deviations of LCE ratios for $\bar{f}_y = 37$ Hz and $T = 8$ s.

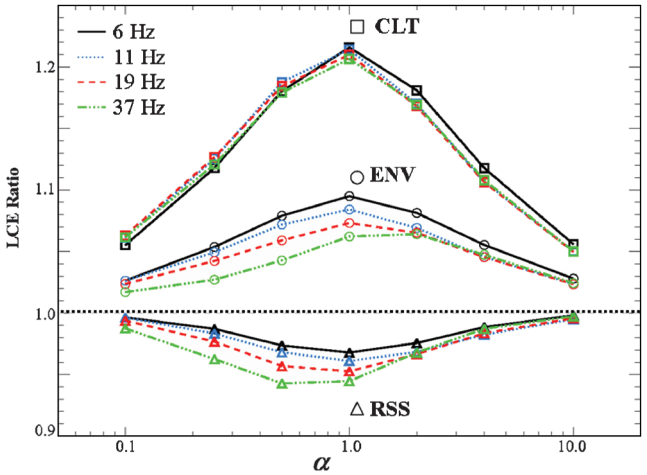


Fig. 7 Frequency-separation effects. Average LCE ratios vs $\alpha$ for $T = 8$ s and $\bar{f}_y = 6$, 11, 19, and 37 Hz.

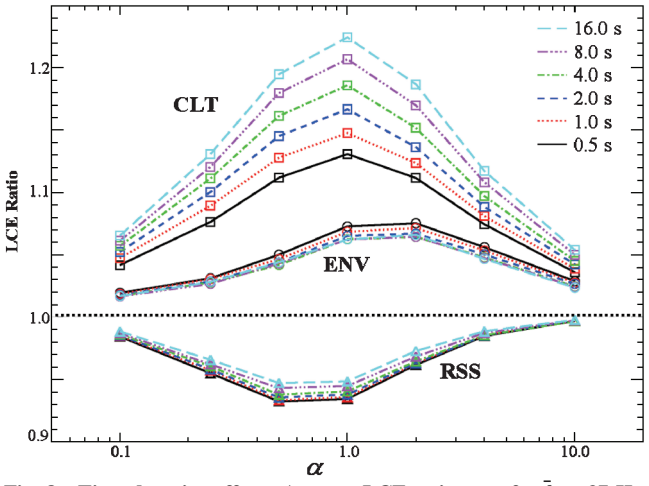


Fig. 8 Time-duration effects. Average LCE ratios vs $\alpha$ for $\bar{f}_y = 37$ Hz and $T = 0.5$, 1, 2, 4, 8, and 16 s.

19, and 37 Hz. Observe that the RSS and ENV LCE ratios decrease with increasing frequency separation for $\alpha \leq 1$: that is, when the higher-frequency response is not dominating. On the other hand, the LCE ratios are less sensitive when either the lower- or higher-frequency responses dominate. The CLT LCE ratios have less variability with respect to frequency separation.

The effects of time duration are shown in Fig. 8. The average LCE ratios vs $\alpha$ for $\bar{f}_y = 37$ Hz, and $T = 0.5$, 1, 2, 4, 8, and 16 s are plotted. The data indicate that, on average, regardless of duration, the RSS LCE underpredicted the desired enclosure level. On the other hand, the ENV LCE and the CLT LCE enveloped the desired levels, with the former providing a more reasonable bounding estimate of the 99/90 levels. Note that the CLT LCE is the most sensitive to time duration and becomes more conservative as $T$ increases. The RSS and ENV forms of the LCE appear to be less sensitive to time duration, with the ENV LCE being the least sensitive.

### Complex System

Monte Carlo simulations that combined loads computed for 950 load parameters, such as moments and shears, of a complex spacecraft system, were performed and the results were compared against loads obtained with the three loads combination equations described previously. The combination involved three distinct types of loads: 1) turbulence/gust, 2) buffet, and 3) engine thrust oscillation. These events were selected because they represent actual loading conditions. Furthermore, turbulence/gust loads have energy content below 10 Hz, thrust-oscillation loads have predominant energy content up to roughly 30 Hz, and low-frequency buffet loads have energy content up to roughly 60 Hz. This provided for a combination of loads with varying frequency content and magnitude. The analyses were performed for the time of flight at which the turbulence/gust loads tend to be highest.

Turbulence/gust loads were computed using 686 turbulence forcing functions. These were developed by extracting the non-persistent rapidly varying features [18–20] from measured wind profiles. The loads were obtained by numerically integrating the coupled system structural dynamic equations of motion that included aeroelastic effects and the launch vehicle control system. Each of the resulting response load time histories was 8 s long. Hence, for each of the 950 load parameters, 686 8-s-long time histories were available for the Monte Carlo simulations.

Buffet loads were computed with 50 30-s-long forcing-function time-history sets. These were developed from power spectral densities that represented the buffet forces acting at various stations along the length of the vehicle. The force time histories were generated by inversely transforming the PSDs and randomizing the phase. No correlation was assumed between the resulting force time histories. The buffet loads were computed in the time domain [21,22] by numerically integrating the equations of motion and using the resulting acceleration and displacement time histories to compute the 950 spacecraft load-parameter time histories. Hence, there were 50 30-s-long time histories for each of the 950 load parameters available for the Monte Carlo analyses.

Thrust-oscillation forcing functions were generated from a family of existing thrust and lateral force time histories that had been

developed from flight data. Similar to the buffet forcing functions, the PSDs of these time histories were calculated, and from these PSDs, 756 sets of 8 s axial and lateral force time histories were synthesized by inverse transformation. The loads were obtained by numerically integrating the coupled system equations of motion and using the resulting acceleration and displacement time histories to compute the 950 spacecraft load-parameter time histories. Therefore, for each of the 950 load parameters, there were 756 8-s-long time histories available for the Monte Carlo simulations.

Let the vector-valued functions $\mathbf{G}(t)$, $\mathbf{TO}(t)$, and $\mathbf{B}(t)$ represent the 950 load time histories for turbulence/gust, thrust oscillation, and buffet, respectively. We shall adhere to the convention of using boldfaced letters to represent vector-valued variables. Each Monte Carlo simulation consisted of 3000 sums of these response time histories, which were randomly drawn from their respective sets of computed responses. For each Monte Carlo draw, load time histories $\mathbf{G}_{i_G}(t)$, $\mathbf{TO}_{i_{\mathrm{TO}}}(t)$, and $\mathbf{B}_{i_B}(t)$ were randomly selected from their sets that contained 686, 756, and 50 cases, respectively. From the selected 30 s buffet response, an 8 s segment, $\mathbf{B}_{i_B,\tau_i}(t)$, was extracted at random. The three 8 s time histories were then summed. Figure 9 illustrates the combination of time histories for the $i$th draw. For each draw, the maximum (and minimum) of the turbulence/gust $\hat{\mathbf{G}}_i$, buffet $\hat{\mathbf{B}}_i$, thrust oscillation $\widehat{\mathbf{TO}}_i$, and total responses $\hat{\mathbf{Z}}_i$ were determined. For the 950 load parameters, the RSS, CLT, and ENV LCEs were calculated using the 99/90 peak responses that were determined by ordered statistics. The means of the maximum (and minimum) responses that were used in the CLT form of the LCE were calculated as

$$\hat{\boldsymbol{\mu}}_{\mathrm{gust}} = \frac{1}{3000}\sum_{i=1}^{3000}\hat{\mathbf{G}}_i, \qquad \hat{\boldsymbol{\mu}}_{\mathrm{TO}} = \frac{1}{3000}\sum_{i=1}^{3000}\widehat{\mathbf{TO}}_i$$

$$\hat{\boldsymbol{\mu}}_{\mathrm{buffet}} = \frac{1}{3000}\sum_{i=1}^{3000}\hat{\mathbf{B}}_i \tag{16}$$

The standard deviations that were used in the ENV form of the LCE were computed from the average root-mean-squared values across all time histories for each event:

$$\boldsymbol{\sigma}_{\mathrm{gust}} = \frac{1}{686}\sum_{i=1}^{686}\boldsymbol{\sigma}_{i,\mathrm{gust}}, \qquad \boldsymbol{\sigma}_{\mathrm{TO}} = \frac{1}{756}\sum_{i=1}^{756}\boldsymbol{\sigma}_{i,\mathrm{TO}}$$

$$\boldsymbol{\sigma}_{\mathrm{buffet}} = \frac{1}{50}\sum_{i=1}^{50}\boldsymbol{\sigma}_{i,\mathrm{buffet}} \tag{17}$$

For each load parameter, the LCEs for the maxima were calculated by (18–20)

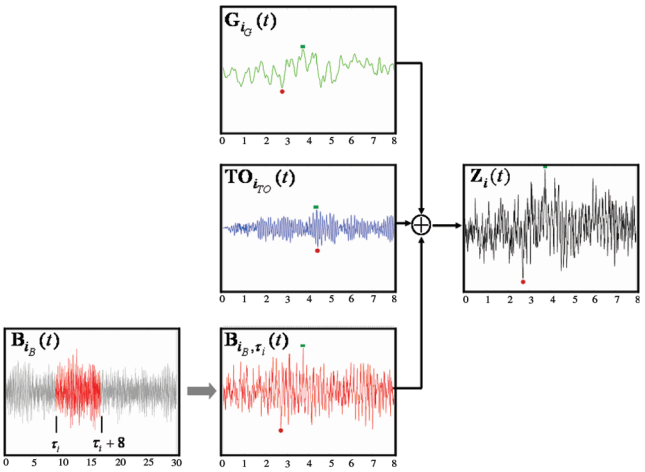


**Fig. 9 Combination of turbulence/gust, thrust-oscillation, and buffet load time histories for one load parameter and the *i*th Monte Carlo draw. For each draw, the maxima and minima of the load contributors and of the total response were determined and recorded for statistical analysis.**

$$\mathrm{RSS}\,(\hat{\mathbf{G}}_{99/90}, \widehat{\mathbf{TO}}_{99/90}, \hat{\mathbf{B}}_{99/90}) = [\hat{\mathbf{G}}^2_{99/90} + \widehat{\mathbf{TO}}^2_{99/90} + \hat{\mathbf{B}}^2_{99/90}]^{1/2} \tag{18}$$

$$\begin{aligned}\mathrm{ENV}(\hat{\mathbf{G}}_{99/90}, \widehat{\mathbf{TO}}_{99/90}, \hat{\mathbf{B}}_{99/90}) &= \sqrt{\frac{\pi}{2}}(\boldsymbol{\sigma}_{\mathrm{gust}} + \boldsymbol{\sigma}_{\mathrm{TO}} + \boldsymbol{\sigma}_{\mathrm{buffet}}) \\ &+ \left[\left(\hat{\mathbf{G}}_{99/90} - \sqrt{\frac{\pi}{2}}\boldsymbol{\sigma}_{\mathrm{gust}}\right)^2 + \left(\widehat{\mathbf{TO}}_{99/90} - \sqrt{\frac{\pi}{2}}\boldsymbol{\sigma}_{\mathrm{TO}}\right)^2\right. \\ &+ \left.\left(\hat{\mathbf{B}}_{99/90} - \sqrt{\frac{\pi}{2}}\boldsymbol{\sigma}_{\mathrm{buffet}}\right)^2\right]^{1/2}\end{aligned} \tag{19}$$

$$\begin{aligned}\mathrm{CLT}(\hat{\mathbf{G}}_{99/90}, \widehat{\mathbf{TO}}_{99/90}, \hat{\mathbf{B}}_{99/90}) &= (\hat{\boldsymbol{\mu}}_{\mathrm{gust}} + \hat{\boldsymbol{\mu}}_{\mathrm{TO}} + \hat{\boldsymbol{\mu}}_{\mathrm{buffet}}) \\ &+ [(\hat{\mathbf{G}}_{99/90} - \hat{\boldsymbol{\mu}}_{\mathrm{gust}})^2 + (\widehat{\mathbf{TO}}_{99/90} - \hat{\boldsymbol{\mu}}_{\mathrm{TO}})^2 \\ &+ (\hat{\mathbf{B}}_{99/90} - \hat{\boldsymbol{\mu}}_{\mathrm{buffet}})^2]^{1/2}\end{aligned} \tag{20}$$

The LCEs for the minima were determined similarly.

Figure 10 presents the ratios of the loads combination equations relative to the Monte Carlo results for each of the 950 load parameters. Observe that the RSS LCE underpredicted approximately half of the load parameters. The ENV LCE resulted in each load parameter being equal to or greater than the Monte Carlo results, with about 15% conservatism on average. The CLT LCE generally yielded higher combined loads than the ENV LCE, bounding the Monte Carlo results by approximately an average of 35%.

To determine if the underprediction by the RSS LCE could be due to the seed used to initiate the Monte Carlo draws, 2 of the 950 load parameters that had an underprediction by the RSS LCE were selected, and the Monte Carlo analyses were repeated 1000 times, each starting with a different seed. To simplify the problem, only the turbulence/gust and thrust-oscillation loads were combined. As can be ascertained from Fig. 11, in which all 1000 cases are plotted, the large majority resulted in the RSS LCE underpredicting the Monte Carlo results.

## Loads-Combination-Equation Analytical Bounds

As a result of the Monte Carlo analyses presented previously, there is strong empirical evidence that the ENV LCE provides, for all practical purposes, a reasonable bound to the desired statistical enclosure levels. On the other hand, the previous results indicate that the RSS LCE often underpredicts the correct total load. The purpose

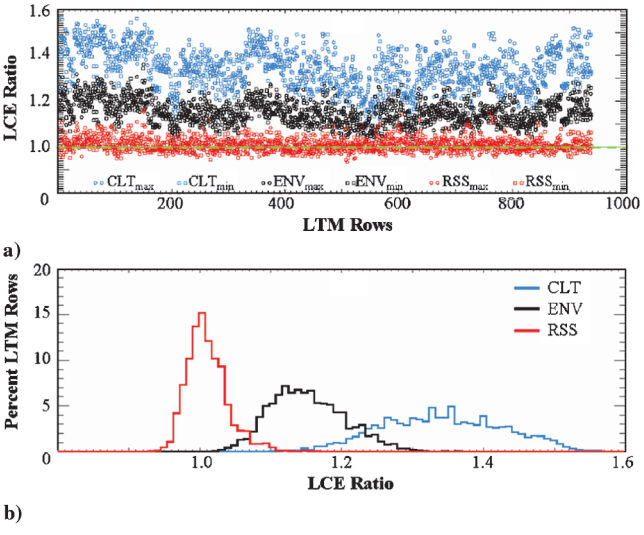


**Fig. 10 Ratios of RSS, env, and CLT LCEs to Monte Carlo results for 950 spacecraft load parameters (load transformation matrix rows): a) maxima and minima results are shown as circles and squares, respectively, and b) histograms of percent of load parameters vs LCE ratio.**

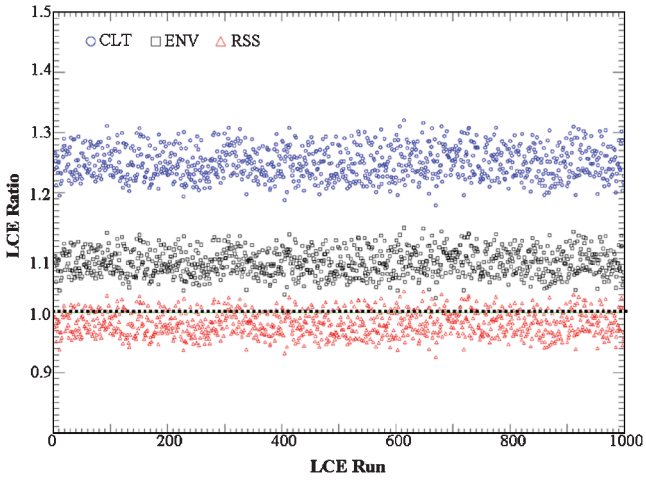


**Fig. 11 LCE ratios vs LCE run from Monte Carlo simulation combining turbulence/gust and thrust-oscillation responses: a) load parameter 1 and b) load parameter 2.**

of this section is to present arguments that establish the bounding properties of the ENV LCE and explain the underpredictions observed with the RSS LCE. We first show that the form of the ENV LCE is based upon summing the envelope functions of the response time series. The arguments show that for the simple systems considered, the RSS LCE and ENV LCE bound, in an instantaneous sense, any enclosure level of the peaks of the total response. Because physical responses must be analyzed over a time period at which load events are predicted to occur, time-duration effects must be accounted for by the LCE bounds. We then discuss how time duration and frequency separation affect the statistics of peaks and explain the properties of the RSS and ENV LCEs observed for simple systems.

Let $x(t)$ and $y(t)$ be zero-mean stationary Gaussian responses with probability density functions

$$f_x(v) = \frac{1}{\sqrt{2\pi}\sigma_x}\exp\left(\frac{-v^2}{2\sigma_x^2}\right), \quad f_y(v) = \frac{1}{\sqrt{2\pi}\sigma_y}\exp\left(\frac{-v^2}{2\sigma_y^2}\right) \tag{21}$$

Because we are interested in combining responses with different relative amplitudes, we shall henceforth assume that $\sigma_x = 1$ and $\sigma_y = \alpha$, where $0 < \alpha < \infty$. Assume that $x(t)$ and $y(t)$ are independent, and let $z(t) = x(t) + y(t)$. Then $z(t)$ has the PDF

$$f_z(v) = \frac{1}{\sqrt{2\pi}\sigma_z}\exp\left(\frac{-v^2}{2\sigma_z^2}\right), \qquad \sigma_z = \sqrt{1+\alpha^2} \tag{22}$$

Consider the Hilbert transform of $x(t)$ defined by the Cauchy principal value (p.v.),

$$x_H(t) = \text{p.v.}\frac{1}{\pi}\int_{-\infty}^{\infty}\frac{x(\tau)}{t-\tau}\,\mathrm{d}\tau \triangleq \lim_{\varepsilon\to 0^+}\frac{1}{\pi}\int_{|t-\tau|>\varepsilon}\frac{x(\tau)}{t-\tau}\,\mathrm{d}\tau \tag{23}$$

Then $x_H(t)$ is also a zero-mean stationary Gaussian process having identical distribution and is uncorrelated to $x(t)$. The envelope function $\tilde{x}(t)$ is then defined by

$$\tilde{x}(t) = \sqrt{x^2(t) + x_H^2(t)} \tag{24}$$

It can be shown [23] that $\tilde{x}(t)$ has the Rayleigh distribution:

$$f_{\tilde{x}}(v) = v\exp\left(\frac{-v^2}{2}\right) \tag{25}$$

Figure 2 shows a typical narrowband response and its envelope function with their respective PDFs plotted vertically along the ordinate axis. Similarly, define the Hilbert transforms $y_H(t)$ and $z_H(t)$ and the associated envelope functions:

$$\tilde{y}(t) = \sqrt{y^2(t) + y_H^2(t)}, \qquad \tilde{z}(t) = \sqrt{z^2(t) + z_H^2(t)} \tag{26}$$

The PDFs of $\tilde{y}(t)$ and $\tilde{z}(t)$ are, respectively,

$$f_{\tilde{y}}(v) = \frac{v}{\alpha^2}\exp\left(\frac{-v^2}{2\alpha^2}\right), \quad f_{\tilde{z}}(v) = \frac{v}{1+\alpha^2}\exp\left(\frac{-v^2}{2(1+\alpha^2)}\right) \tag{27}$$

The mean and variance of these Rayleigh distributions are given by [15]

$$\mu_{\tilde{x}} = \sqrt{\frac{\pi}{2}}, \qquad \mu_{\tilde{y}} = \sqrt{\frac{\pi}{2}}\alpha, \qquad \mu_{\tilde{z}} = \sqrt{\frac{\pi}{2}}\sqrt{1+\alpha^2}$$
$$\text{var}\{\tilde{x}\} = \frac{4-\pi}{2}, \qquad \text{var}\{\tilde{y}\} = \frac{4-\pi}{2}\alpha^2$$
$$\text{var}\{\tilde{z}\} = \frac{4-\pi}{2}(1+\alpha^2) \tag{28}$$

Integrating the Rayleigh PDFs leads to the following distributions for $\tilde{x}(t)$, $\tilde{y}(t)$, and $\tilde{z}(t)$:

$$F_{\tilde{x}}(v) = 1 - \exp\left(\frac{-v^2}{2}\right), \qquad F_{\tilde{y}}(v) = 1 - \exp\left(\frac{-v^2}{2\alpha^2}\right)$$
$$F_{\tilde{z}}(v) = 1 - \exp\left(\frac{-v^2}{2(1+\alpha^2)}\right) \tag{29}$$

Hence, for a specified enclosure probability $p$, Eq. (29) leads to the $p$ quantiles:

$$\tilde{X}_p = F_{\tilde{x}}^{-1}(p) = \xi_p, \qquad \tilde{Y}_p = F_{\tilde{y}}^{-1}(p) = \alpha\xi_p$$
$$\tilde{Z}_p = F_{\tilde{z}}^{-1}(p) = \sqrt{1+\alpha^2}\xi_p \tag{30}$$

where $\xi_p = \sqrt{-2\ln(1-p)}$.

Now introduce the sum of the envelopes, $u(t) = \tilde{x}(t) + \tilde{y}(t)$. By virtue of independence,

$$\mu_u = \sqrt{\frac{\pi}{2}}(1+\alpha), \qquad \text{var}\{u\} = \frac{4-\pi}{2}(1+\alpha^2) \tag{31}$$

Also, independence of $\tilde{x}(t)$ and $\tilde{y}(t)$ allows us to calculate the PDF of $u(t)$:

$$f_u(v) = f_{\tilde{x}} * f_{\tilde{y}}(v) = \int_0^v f_{\tilde{x}}(v-r)f_{\tilde{y}}(r)\,\mathrm{d}r$$
$$= \frac{1}{\alpha^2}\int_0^v r(v-r)\exp\left[\frac{-r^2}{2\alpha^2} + \frac{-(v-r)^2}{2}\right]\mathrm{d}r \tag{32}$$

The distribution function of $u(t)$ is then obtained by direct integration:

$$F_u(v) = \int_0^v f_u(s)\,\mathrm{d}s = 1 - e^{-v^2/2\alpha^2} - \frac{e^{-v^2/2} - e^{-v^2/2\alpha^2}}{1+\alpha^2} - \sqrt{\frac{\pi}{2}}\frac{\alpha v}{(1+\alpha^2)^{3/2}} e^{-v^2/2(1+\alpha^2)}\left[\mathrm{erf}\left(\frac{\alpha v}{\sqrt{2(1+\alpha^2)}}\right) + \mathrm{erf}\left(\frac{\alpha^{-1} v}{\sqrt{2(1+\alpha^2)}}\right)\right] \tag{33}$$

where

$$\mathrm{erf}\,(v) = \frac{2}{\sqrt{\pi}}\int_0^v e^{-s^2}\,\mathrm{d}s$$

Therefore, we can represent the $p$ quantile for $u(t)$ by the usual mean plus $k$-sigma form:

$$U_p = F_u^{-1}(p) = \mu_u + k_p(\alpha)\sqrt{\mathrm{var}\{u\}} = \sqrt{\frac{\pi}{2}}(1+\alpha) + k_p(\alpha)\sqrt{\frac{4-\pi}{2}}\sqrt{1+\alpha^2} \tag{34}$$

where the factor $k_p(\alpha)$ is defined implicitly.

Observe that the triangle inequality implies that the envelope of the sum is less than or equal to the sum of the envelopes; that is,

$$\tilde{z}(t) \le \tilde{x}(t) + \tilde{y}(t) = u(t) \tag{35}$$

Therefore, we obtain the following inequality involving the distributions:

$$F_{\tilde{z}}(\xi) \ge F_u(\xi), \qquad \xi \ge 0 \tag{36}$$

This is a direct consequence of Eq. (35) and monotonicity, which imply

$$\{\tilde{z} \le \xi\} \supseteq \{u \le \xi\} \Rightarrow \mathrm{prob}\{\tilde{z} \le \xi\} \ge \mathrm{prob}\{u \le \xi\} \tag{37}$$

Hence, we obtain the following inequality for the $p$ quantiles:

$$U_p \ge \tilde{Z}_p \tag{38}$$

Figure 12 illustrates the inequalities in Eqs. (36) and (38).

For an enclosure probability $p$, the ENV form of the LCE, proposes that we add the means and root-sum-square the dispersed terms:

$$\mathrm{ENV}(\tilde{X}_p, \tilde{Y}_p) = (\mu_{\tilde{x}} + \mu_{\tilde{y}}) + [(\tilde{X}_p - \mu_{\tilde{x}})^2 + (\tilde{Y}_p - \mu_{\tilde{y}})^2]^{1/2} = \sqrt{\frac{\pi}{2}}(1+\alpha) + \left|\xi_p - \sqrt{\frac{\pi}{2}}\right|\sqrt{1+\alpha^2} \tag{39}$$

We claim that

$$\mathrm{ENV}\,(\tilde{X}_p, \tilde{Y}_p) > U_p \tag{40}$$

Comparing Eqs. (34) and (39), it suffices to show that for $0 < \alpha \le 1$,

$$\left|\xi_p - \sqrt{\frac{\pi}{2}}\right| > k_p(\alpha)\sqrt{\frac{4-\pi}{2}} \tag{41}$$

The preceding inequality was verified numerically for $0 \le p \le 0.999$ and $0 < \alpha \le 1$ in 0.001 increments. Figure 13 shows that for each $p$, $|\xi_p - \sqrt{\pi/2}|$ is equal to the maximum of $k_p(\alpha)\sqrt{(4-\pi)/2}$ over $\alpha$, which occurs when $\alpha \to 0$.

The incorporation of the statistics of the response peaks into the LCE estimates requires us to relate the Rayleigh distribution to that of the peaks. It is well known that the peaks of a narrowband response will have a Rayleigh distribution, whereas those for a broadband response will have a distribution that tends toward normal. This

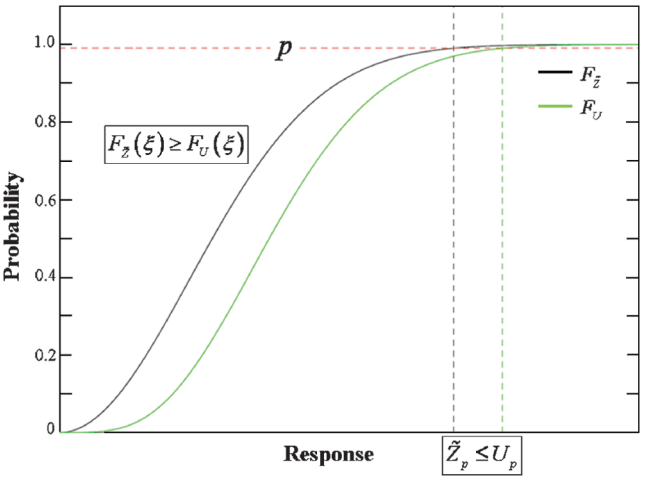


**Fig. 12 Distribution functions of $\tilde{z}(t)$ and $u(t)$ and the corresponding $p$ quantiles.**

statement was made precise by Cartwright and Longuet–Higgins [24], who extended the work of Rice [25] and determined the probability distributions of peaks for a stationary random process.

Let $z(t)$ be a stationary Gaussian process with root mean square $\sigma_z = \sqrt{m_0}$. Then the probability distribution of its normalized maxima, $v = \hat{z}/\sigma_z$, is given by

$$f_{\hat{z}}(v) = \frac{\varepsilon}{\sqrt{2\pi}} e^{\frac{-v^2}{2\varepsilon^2}} + \frac{\sqrt{1-\varepsilon^2}}{2} v e^{\frac{-v^2}{2}}\left[1 + \mathrm{erf}\left(\frac{v\sqrt{1-\varepsilon^2}}{\sqrt{2}\varepsilon}\right)\right], \quad 0 \le \varepsilon \le 1 \tag{42}$$

where $\varepsilon$ is a measure of spectral width and is defined in terms of the moments of the PSD, $G_z(\omega)$:

$$\varepsilon^2 = 1 - \frac{m_2^2}{m_0 m_4}, \qquad m_k = \int_0^\infty \omega^k G_z(\omega)\,\mathrm{d}\omega \tag{43}$$

Integrating Eq. (42) yields the cumulative distribution function:

$$F_{\hat{z}}(v) = \frac{1}{2}\left\{1 + \mathrm{erf}\left(\frac{v}{\sqrt{2}\varepsilon}\right) - \sqrt{1-\varepsilon^2} e^{-\frac{v^2}{2}}\left[1 + \mathrm{erf}\left(\frac{v\sqrt{1-\varepsilon^2}}{\sqrt{2}\varepsilon}\right)\right]\right\} \tag{44}$$

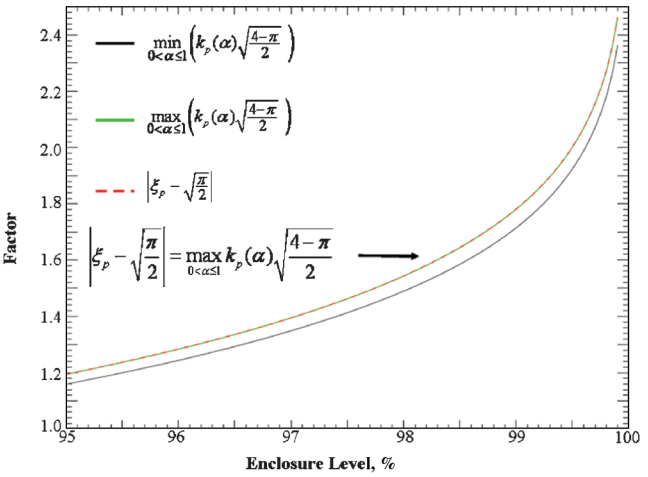


**Fig. 13 Comparison of factors for the dispersed terms for $\mathrm{ENV}(\tilde{X}_p, \tilde{Y}_p)$ and $U_p$.**

Figure 14 plots $f_z(v)$ and $F_z(v)$ for several values of $\varepsilon$. Note that $\varepsilon$ values of 0 and 1 correspond to Rayleigh and Gaussian distributions, respectively.

Equations (42) and (44) describe the statistics of the maxima $\hat{z}$, which include both positive and negative maxima. However, to assess peak loads, the positive maxima and negative minima must be considered separately. For the purposes of this discussion, we will assume symmetry of the extrema and determine the probability distribution for the positive maxima. Let $\hat{z}^+$ denote the positive maxima, then

$$f_{\hat{z}^+}(v) = \frac{f_{\hat{z}}(v)}{\text{prob}(\hat{z} \geq 0)} = \frac{f_{\hat{z}}(v)}{1 - F_{\hat{z}}(0)} = \frac{2}{1 + \sqrt{1 - \varepsilon^2}} f_{\hat{z}}(v)$$

$$v \geq 0$$

$$F_{\hat{z}^+}(v) = \frac{2}{1 + \sqrt{1 - \varepsilon^2}} [F_{\hat{z}}(v) - F_{\hat{z}}(0)]$$

$$= \frac{2}{1 + \sqrt{1 - \varepsilon^2}} \left[ F_{\hat{z}}(v) - \frac{1 - \sqrt{1 - \varepsilon^2}}{2} \right] \tag{45}$$

Figure 15 plots $f_{\hat{z}^+}(v)$ and $F_{\hat{z}^+}(v)$ for several values of $\varepsilon$. Observe that the Rayleigh distribution is bounding in the sense that it yields larger $p$ quantiles than any of the positive maxima distributions; that is,

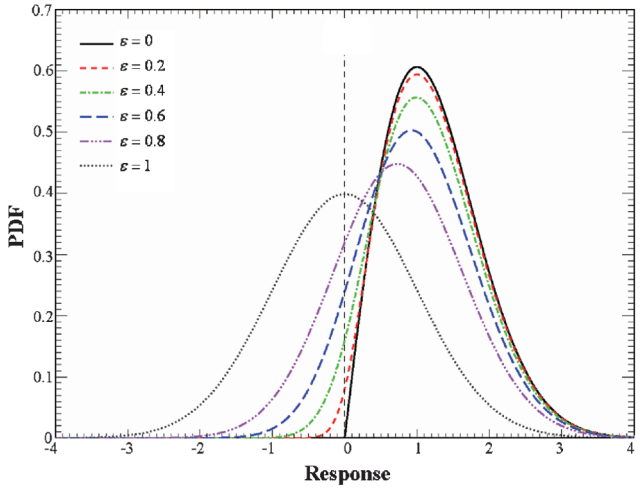


a)

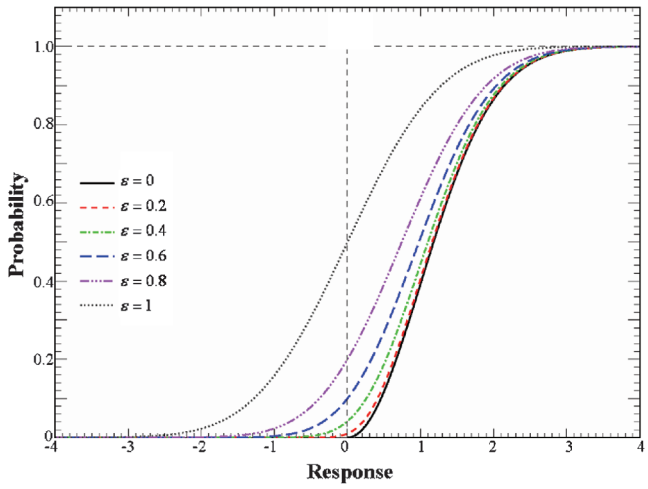


b)

**Fig. 14 Distribution of maxima: a) probability density function and b) cumulative distribution function.**

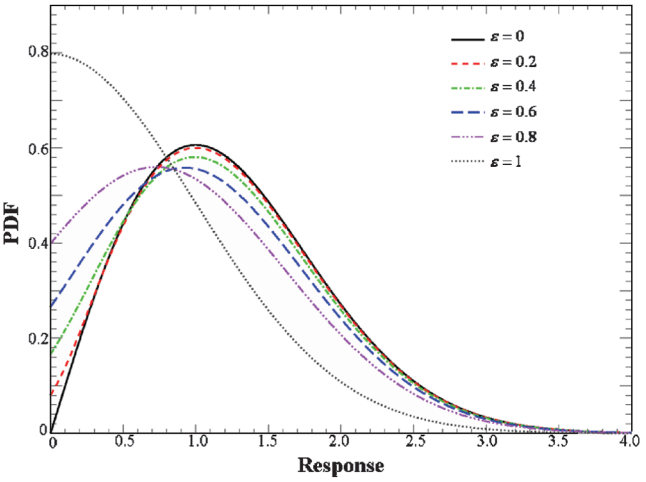


a)

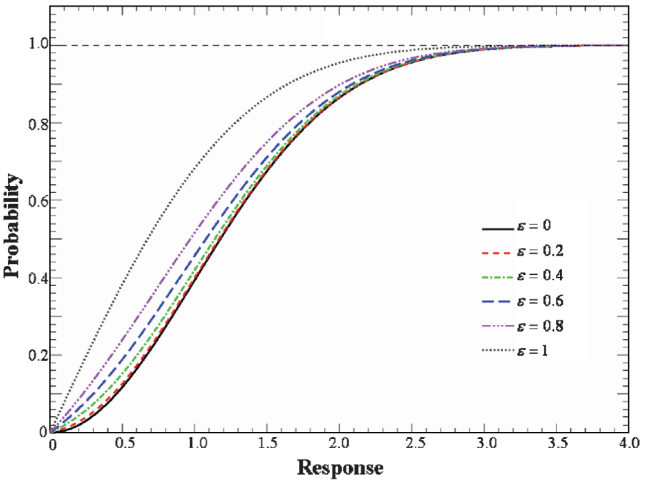


b)

**Fig. 15 Distribution of positive maxima: a) probability density function and b) cumulative distribution function.**

$$\tilde{Z}_p \geq \hat{Z}_p^+ = \sigma_z F_{\hat{Z}^+}^{-1}(p) \tag{46}$$

We verified Eq. (46) on a multimode response for which the PSD (normalized to unit mean square) is shown in Fig. 16a. We calculated the envelope function and identified the peaks for a 1000 s, zero-mean, Gaussian time series $z(t)$ that was synthesized from the PSD. Figure 16b shows a portion of $z(t)$, its envelope function, maxima, and positive maxima. As shown in Fig. 17, the histogram estimates of the distributions of $\tilde{z}(t)$, $\hat{z}$, and $\hat{z}^+$ compare well with their respective theoretical functions.

Together, Eqs. (38), (40), and (46) imply the following chain of inequalities:

$$\text{ENV}(\tilde{X}_p, \tilde{Y}_p) > U_p \geq \tilde{Z}_p \geq \hat{Z}_p^+ \tag{47}$$

Equation (47) establishes the bounding property for the ENV form of the LCE. Additionally, by Eqs. (30) and (46), we have

$$\text{RSS}(\tilde{X}_p, \tilde{Y}_p) = \tilde{Z}_p \geq \hat{Z}_p^+ \tag{48}$$

Moreover, if $x(t)$ and $y(t)$ are responses of SDOF systems, then $\hat{x}^+$ and $\hat{y}^+$ will essentially be Rayleigh-distributed, and

$$\tilde{X}_p \approx \hat{X}_p^+, \qquad \tilde{Y}_p \approx \hat{Y}_p^+ \tag{49}$$

Therefore, Eqs. (47) and (48) yield the inequality

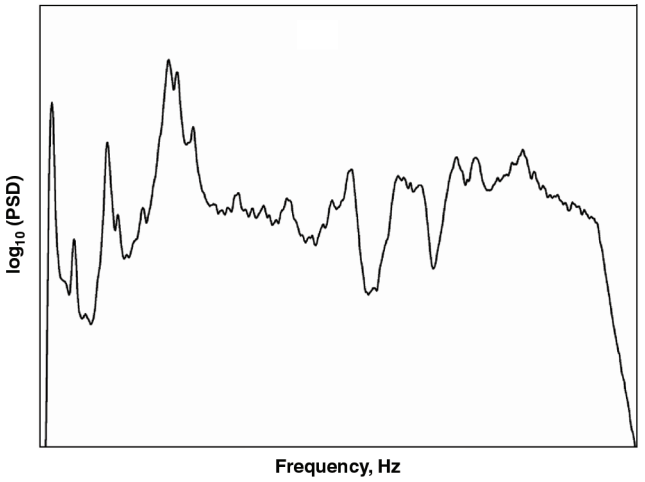


a)

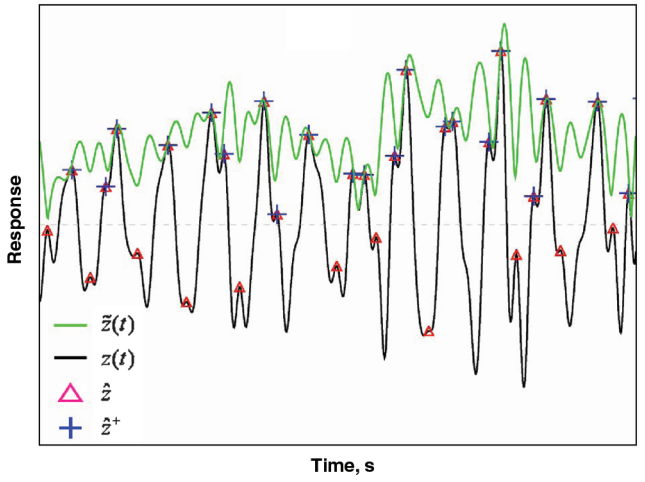


b)

**Fig. 16 Multimode response: a) PSD and b) close-up of time series, envelope function, maxima, and positive maxima.**

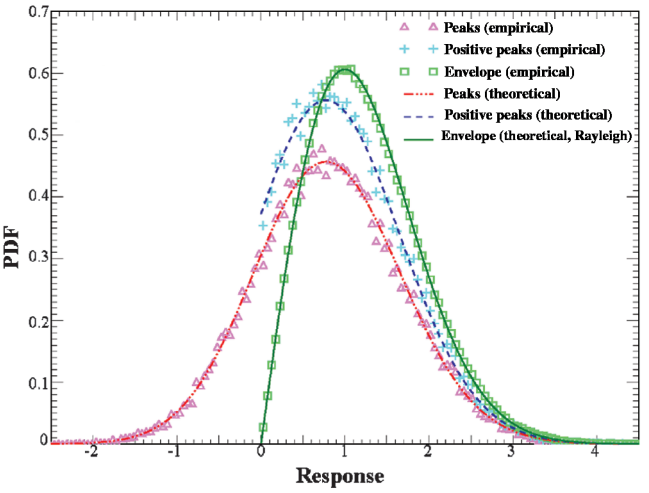


a)

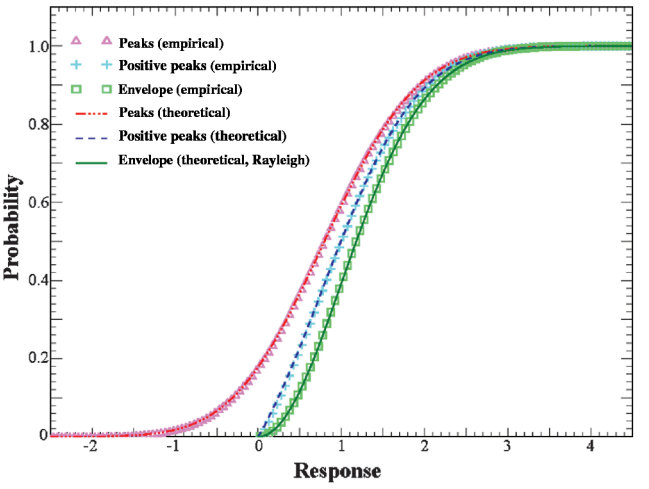


b)

**Fig. 17 Distribution functions of envelope function, maxima, and positive maxima of a multimode response: a) probability density function and b) cumulative distribution function.**

$$\text{ENV}(\hat{X}_p^+, \hat{Y}_p^+) > \text{RSS}(\hat{X}_p^+, \hat{Y}_p^+) \geq \hat{Z}_p^+ \tag{50}$$

that establishes the bounding properties of the RSS LCE and ENV LCE for the instantaneous combination of responses. Note the subtle implication of Eq. (50) that asserts that the ENV LCE will strictly bound any enclosure level of $\hat{z}^+$.

The Monte Carlo analyses for simple systems demonstrated that whereas the ENV LCE bound remained in force for various time durations and frequency separations, the RSS LCE bound did not. This is because the instantaneous estimates do not account for the statistics of multiple peaks that depend upon duration, frequency, and correlation, due to the physical properties of the system.

For a given time duration $T$, the expected number of positive maxima is given by [24,25]

$$N^+ = \left(\frac{1+\sqrt{1-\varepsilon^2}}{4\pi}\sqrt{\frac{m_4}{m_2}}\right)\cdot T \tag{51}$$

Let $N_x^+$ represent the expected number of positive maxima in a duration $T$ for $\hat{x}^+$. For simplicity, assume that the peaks are independent. Then the distribution of the largest positive peak $\hat{x}_{\max}^+$ is defined by

$$F_{\hat{X}_{\max}^+}(v) = [F_{\hat{X}^+}(v)]^{N_x^+} \tag{52}$$

Hence, the quantile corresponding to an enclosure probability $p$ is

$$\hat{X}^+_{\max,p} = \sigma_x F^{-1}_{\hat{X}^+}(p^{\frac{1}{N_x^+}}) \tag{53}$$

Similarly, the $p$ quantiles for $\hat{y}_{\max}^+$ and $\hat{z}_{\max}^+$ are given by

$$\hat{Y}^+_{\max,p} = \sigma_y F^{-1}_{\hat{Y}^+}(p^{\frac{1}{N_y^+}}), \qquad \hat{Z}^+_{\max,p} = \sigma_z F^{-1}_{\hat{Z}^+}(p^{\frac{1}{N_z^+}}) \tag{54}$$

We now evaluate $\text{RSS}(\hat{X}^+_{\max,p}, \hat{Y}^+_{\max,p})$ and $\text{ENV}(\hat{X}^+_{\max,p}, \hat{Y}^+_{\max,p})$ for a simple system, where $x(t)$ and $y(t)$ are narrowband responses about frequencies $\bar{f}_x$ and $\bar{f}_y$, respectively, and with bandwidth equal to $\Delta f$. As in the Monte Carlo simulation with the simple systems, we shall assume that $\bar{f}_y \geq \bar{f}_x$ and that $\sigma_x = 1$ and $\sigma_y = \alpha$, with $0 < \alpha < \infty$. Let $r_y = \bar{f}_y/\bar{f}_x$ denote the frequency ratio. If $\Delta f \ll 1$, then $\hat{x}^+$ and $\hat{y}^+$ are essentially Rayleigh-distributed and, moreover, $N_x^+ \approx T\bar{f}_x$ and $N_y^+ \approx r_y N_x^+$. Hence,

$$\hat{X}^+_{\max,p} \approx \sqrt{-2\,\ell n(1-p^{\frac{1}{N_x^+}})}, \qquad \hat{Y}^+_{\max,p} \approx \alpha\sqrt{-2\,\ell n(1-p^{\frac{1}{r_y N_x^+}})} \tag{55}$$

Calculating the spectral moments of $z(t) = x(t) + y(t)$ yields, after neglecting the $\Delta f^2$ terms, the $\varepsilon$ parameter that describes the distribution of $\hat{z}$,

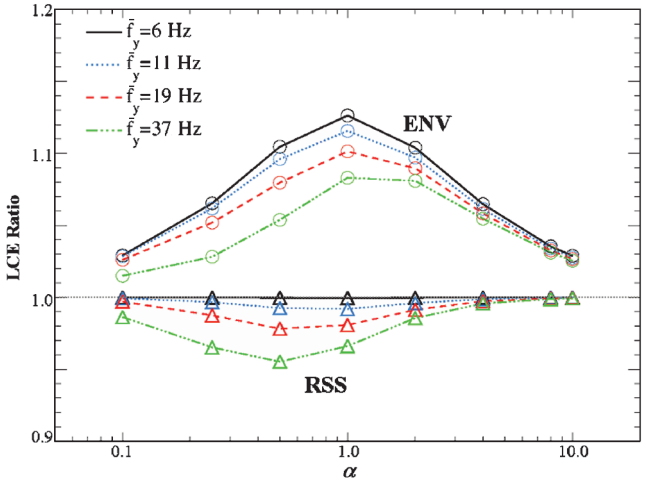


**Fig. 18 Theoretical LCE ratios vs $\alpha$ for $T = 8$ s, $\bar{f}_x = 5$ Hz, and $\bar{f}_y = 6$, 11, 19, and 37 Hz.**

$$\varepsilon^2 \approx \frac{\alpha^2}{1+\alpha^2} \cdot \frac{(r_y^2 - 1)^2}{1 + \alpha^2 r_y^4} \tag{56}$$

and also the expected number of positive maxima $\hat{z}^+$,

$$N_z^+ \approx \left( \frac{1 + \sqrt{1-\varepsilon^2}}{2} \sqrt{\frac{1+\alpha^2 r^4}{1+\alpha^2 r^2}} \right) \cdot N_x^+ \equiv r_z N_x^+ \tag{57}$$

Therefore, we obtain the $p$ quantile for $\hat{z}^+_{\max}$ over the duration $T$:

$$\hat{Z}^+_{\max,p} \approx \sqrt{1+\alpha^2} F^{-1}_{\hat{Z}^+}(p^{\frac{1}{r_z N_x^+}}) \tag{58}$$

Using Eqs. (55–58), the LCE ratios

$$r_{\mathrm{RSS}} = \frac{\mathrm{RSS}(\hat{X}^+_{\max,p}, \hat{Y}^+_{\max,p})}{\hat{Z}^+_{\max,p}}, \qquad r_{\mathrm{ENV}} = \frac{\mathrm{ENV}(\hat{X}^+_{\max,p}, \hat{Y}^+_{\max,p})}{\hat{Z}^+_{\max,p}} \tag{59}$$

were calculated for $p = 0.99$; $\bar{f}_x = 5$ Hz; $\bar{f}_y = 6$, 11, 19, and 37 Hz; and $T = 8$ s as a function of $\alpha = 0.1$, 0.25, 0.5, 1, 2, 4, and 10. The ratios are shown in Fig. 18. Observe that the analytical approximation, which does not account for correlation between peaks due to the physical properties of the systems, does a good job of predicting the general behavior of the empirical LCE ratios shown in Fig. 7.

## Conclusions

Three combination equations were assessed by means of Monte Carlo simulations of simple systems and a complex spacecraft and by mathematical analysis that provides insight and more rigor to the conclusions developed from the numerical simulation results. It was demonstrated that the equation that is based on the sum of the envelope functions of the response time histories provides, for all practical purposes, a reasonable bound of the total. The form of the equation that most nearly follows the central limit theorem provides a more conservative estimate than that obtained with the envelope functions. It was also shown that the form of the equation in which all contributors are root-sum-squared frequently underpredicts the desired total. Therefore, it is concluded that the root-sum-squared combination of independent contributors obtained from time-history responses is not appropriate and that the envelope-function form of the combination equation should be used.

## Appendix: Envelope-Function Calculation

The procedure used to calculate the envelope functions of time histories is summarized herein. Let $x(t)$ be a zero-mean band-limited signal with Hilbert transform $x_H(t)$. Then the analytic signal $z(t) = x(t) + ix_H(t)$ has Fourier transform [26]:

$$Z(\omega) = \begin{cases} 2X(\omega), & \omega > 0 \\ X(0), & \omega = 0 \\ 0, & \omega < 0 \end{cases}$$

where $Z(\omega)$ and $X(\omega)$ are the Fourier transforms of $z(t)$ and $x(t)$, respectively. Moreover, the complex modulus of $z(t)$ is equal to the envelope function $\tilde{x}(t)$.

For a sampling period $T_s$, let $x(t_n)$, where $t_n = nT_s$ $(n = 0, \ldots, N-1)$ denotes the discrete signal corresponding to $x(t)$. We shall assume that $N$ is even. The envelope-function calculation is based upon computing the discrete analog of the continuous analytic signal $z(t)$ as described by Marple [26]:

$$Z_m = \begin{cases} X_0, & m = 0 \\ 2X_m, & 1 \le m < \frac{N}{2} \\ X_{N/2}, & m = \frac{N}{2} \\ 0, & \frac{N}{2} < m \le N-1 \end{cases}$$

where $X_m$ is the $m$th discrete Fourier transform coefficient of $x(t_n)$:

$$X_m = \frac{1}{N} \sum_{n=0}^{N-1} x(t_n) \exp\left(-i \frac{2\pi n m}{N}\right)$$

The discrete analytic signal is then defined by the inverse Fourier transform:

$$z(t_n) = \sum_{n=0}^{N-1} Z_m \exp\left(i \frac{2\pi n m}{N}\right)$$

which yields the discrete envelope function $\tilde{x}(t_n) = |z(t_n)|$.

## References

[1] Fleming, E. R., "Spacecraft and Launch Vehicle Loads," *Flight Vehicle Materials, Structures, and Dynamics*, Vol. 1, American Society of Mechanical Engineers, New York, Mar. 1991, Chap. 6.

[2] Kabe, A. M., "Design and Verification of Launch and Space Vehicle Structures," AIAA Paper 98-1718, Apr. 1998.

[3] Dotson, K. W., Womack, J. M., and Grosserode, P. J., "Structural Dynamic Analysis of Solid Rocket Motor Resonant Burning," *Journal of Propulsion and Power*, Vol. 17, No. 2, 2001, pp. 347–354. doi:10.2514/2.5748

[4] Ryan, R. S., Scoggins, J. R., and King, A., "Use of Wind Shears in the Design of Aerospace Vehicles," *Journal of Spacecraft and Rockets*, Vol. 4, No. 11, 1967, pp. 1526–1532. doi:10.2514/3.29123

[5] Adelfang, S. I., Smith, O. E., Batts, G. W., and Hill, C. K., "Winds Aloft Statistical Analysis in Support of Day-of-Launch Shuttle Systems Evaluation," AIAA Paper 88-0294, Jan. 1988.

[6] Kabe, A. M., Spiekermann, C. E., Kim, M. C., and Lee, S. S., "A Refined and Less Conservative Day-of-Launch Atmospheric Flight Loads Analysis Approach," *Journal of Spacecraft and Rockets*, Vol. 37, No. 4, 2000, pp. 453–458. doi:10.2514/2.3604

[7] Smith, O. E., and Adelfang, S. I., "On the Relationship Between Wind Profiles and the STS Ascent Structural Loads," AIAA Paper 89-0709, Jan. 1989.

[8] Smith, O. E., Adelfang, S. I., and Batts, G., "Wind Models for the NSTS Ascent Trajectory Biasing for Wind Load Alleviation," AIAA Paper 90-0481, Jan. 1990.

[9] Strauch, R. G., Merritt, D. A., Moran, K. P., May, P. T., Weber, B. L., and Wuertz, D. A., "Doppler Radar Wind Profilers for Support of Flight Operations," AIAA Paper 89-0713, Jan. 1989.

[10] Binkley, J. F., Clarke, J. B., and Spiekermann, C. E., "Improved Procedure for Combining Day-of-Launch Atmospheric Flight Loads," *Journal of Spacecraft and Rockets*, Vol. 37, No. 4, July–Aug. 2000, pp. 459–462. doi:10.2514/2.3605

[11] Macheske, V. M., Womack, J. M., and Binkley, J. F., "A Statistical Technique for Combining Launch Vehicle Atmospheric Flight Loads," AIAA Paper 93-0755, Jan. 1993.

[12] Norbraten, G. L., "Day-of-Launch I-Load Updates for the Space Shuttle," AIAA Paper 92-1274, Mar. 1992.
[13] Spiekermann, C. E., and Kabe, A. M., "Statistical Combination of Launch Vehicle Gust and Buffet Atmospheric Flight Loads," AIAA Paper 98-2010, Apr. 1998.
[14] Houbolt, J. C., "Combining Ascent Loads, NASA Space Vehicle Design Criteria (Structures)," NASA SP-8099, May 1972.
[15] Papoulis, A., *Probability, Random, and Stochastic Processes*, 2nd ed., McGraw–Hill, New York, 1984.
[16] Hurty, W. C., and Rubinstein, M. F., *Dynamics of Structures*, Prentice–Hall, Upper Saddle River, NJ, 1964.
[17] Crandall, S. H., and Mark, W. D., *Random Vibration in Mechanical Systems*, Academic Press, Orlando, FL, 1963.
[18] Spiekermann, C. E., Sako, B. H., and Kabe, A. M., "Identifying Slowly Varying and Turbulent Wind Features for Day-of-Launch Flight Loads Analyses," *Journal of Spacecraft and Rockets*, Vol. 37, No. 4, 2000, pp. 426–433.
doi:10.2514/2.3598
[19] Sako, B. H., Kim, M. C., Kabe, A. M., and Yeung, W. K., "Derivation of Forcing Functions for Monte Carlo Atmospheric Gust Loads Analysis," *Journal of Spacecraft and Rockets*, Vol. 37, No. 4, 2000, pp. 434–442.
doi:10.2514/2.3601
[20] Kim, M. C., Kabe, A. M., and Lee, S. S., "Atmospheric Flight Gust Loads Analysis," *Journal of Spacecraft and Rockets*, Vol. 37, No. 4, 2000, pp. 446–452.
doi:10.2514/2.3603
[21] Kabe, A. M., "Multi-Shaker Random Mode Testing," *Journal of Guidance, Control, and Dynamics*, Vol. 7, No. 6, Nov.–Dec. 1984, pp. 740–746.
doi:10.2514/3.19921
[22] Broussinos, P., and Kabe, A. M., "Multi-Mode Random Response Analysis Procedure," The Aerospace Corp., TR SSD-TR-90-53, Los Angeles, 1990.
[23] Papoulis, A., *Signal Analysis*, 1st ed., McGraw–Hill, New York, 1977.
[24] Cartwright, D. E., and Longuet-Higgins, M. S., "The Statistical Distribution of the Maxima for a Random Function," *Proceedings of the Royal Society of London, Series A: Mathematical and Physical Sciences*, Vol. 237, No. 1209, 1956, pp. 212–232.
doi:10.1098/rspa.1956.0173
[25] Rice, S. O., "Mathematical Analysis of Random Noise," *Bell System Technical Journal* Vol. 23, No. 282, 1944, pp. 51–67.
[26] Marple, S. L., "Computing the Discrete-Time Analytic Signal via FFT," *IEEE Transactions on Signal Processing*, Vol. 47, No. 9, Sept. 1999, pp. 2600–2603.
doi:10.1109/78.782222

J. Samareh
*Associate Editor*